Appl Phys A (2011) 103: 167–172
DOI 10.1007/s00339-010-6036-y

Applied Physics A
Materials Science & Processing

Controlled assembly of poly(vinyl pyrrolidone) fibers through an electric-field-assisted electrospinning method

Xiaojie Cui · Luming Li · Fu Xu

Received: 1 April 2010 / Accepted: 25 August 2010 / Published online: 11 September 2010

Abstract In this paper, we develop an effective electric-field-assisted electrospinning method for the controlled deposition of poly(vinyl pyrrolidone) fibers. The electric field distribution becomes uniform and convergent due to the introduction of a metal plate and a focusing aid into the conventional electrospinning setup. As a result, the bending instability is suppressed and the jet is restricted to moving to the collector along a straight line. Helical structure of fibers with lateral width of about 10 μm is formed and aligned on a rotating substrate. The morphology of helical fibers can also be effectively adjusted by varying the collecting velocity.

1 Introduction

The electrospinning technique has been widely investigated in the past decade as a low-cost and simple method to produce polymeric, ceramic and composite microfibers and nanofibers for a wide range of applications [1–4]. In a typical electrospinning process, when the high voltage is applied to the spinneret-plate system, a jet is ejected from the tip of spinneret and rapidly accelerated from the spinneret towards the substrate by the stretching of electrostatic force. When the jet undergoes a slight perturbation, the repulsive coulomb forces push the jet away from the central axis of the straight jet path and finally change the jet path from a straight line to a conical envelope [5, 6]. This phenomenon is known as the bending instability and exits in the whole course of the fiber formation, so the produced electrospun fibers are usually deposited on the substrate in the form of nonwoven mats [7]. However, the inability of the controllable arrangement of the electrospun fibers limits their extensive functionality [8]. If the bending instability is restricted and the deposition of fibers is controlled, the applications of the electrospun fibers will be extended in many fields, such as optics, electronics, tissue engineering and biomedical sensors [9–11]. Hence it is a significant research topic to control the jet trajectory and generate controllable arrangement of the electrospun fibers. In recent years, some researchers have focused on this issue and many methods are brought forward to solve this problem [12]. For instance, a good alignment of the electrospun fibers is achieved by changing the configurations of the collectors [13–17] or adding assistant electrodes [18, 19] to the electrospinning setups. Besides, ordered two-dimensional and three-dimensional architectures of the electrospun fibers are fabricated when the collecting substrates are replaced by the patterned conductive collectors or 3D tubular structures [20–22]. In order to obtain orderly deposition of the nanofibers, a near-field electrospinning method is developed and it emerges good feasibility in the controllable deposition of ordered nanofiber patterns [23–25]. The electric field can also be manipulated to control the jet trajectory and the fiber alignment. Bias and focusing electrodes [26–28] have been added to the electrospinning setup to form specific distributions of the electric field. As a result, the depositing area of mats is greatly suppressed in the electrospinning process and ordered arrangement or patterning of nanofibers is gained. The shadow mask is also used to change the contribution of the electrostatic field near the depositing position [29]. As a result, the deposi-

X.J. Cui
Department of Mechanical Engineering, Tsinghua University, Beijing, 100084, P.R. China

L.M. Li (✉) · F. Xu
School of Aerospace, Tsinghua University, Beijing 100084, P.R. China
e-mail: lilm@tsinghua.edu.cn
Fax: +86-10-62785716

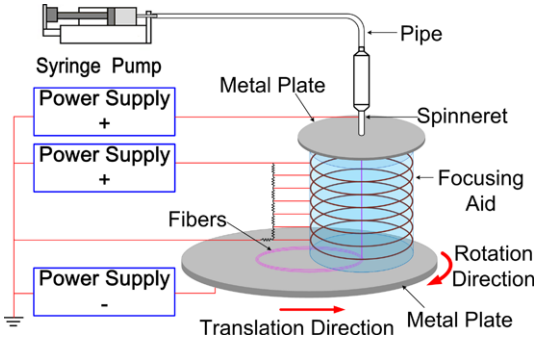

Fig. 1 Schematic diagram of the focusing electric-field-assisted electrospinning setup

tion of electrospun nanofibers is controlled and the sizes of the fiber spots are limited to a few dozen microns. Although a variety of novel structures of the electrospun fibers are fabricated by the mentioned methods, the development of new effective methods based on electrospinning to produce precisely controlled fibrous structures is still a challenge.

In this study, a low-cost and efficient electrospinning method based on the modification of the electric field distribution has been developed for the controlled arrangement of the PVP fibers. A metal plate and a focusing aid are successively introduced to the conventional electrospinning setup to change the distribution of the electric field. A specific electric field, which is uniformed at the initiating region and convergent at the lower part, is finally formed. As a result, the bending instability of jet is suppressed on the moving path because of the fixation of the convergent electric field force and helical structure of fibers with fine lateral width is obtained.

2 Experimental

The schematic setup used in the electrospinning process is shown in Fig. 1. Different from the conventional electrospinning setup, a metal plate with a diameter of 100 mm was placed above the tip of spinneret and welded together with the spinneret. Moreover, a focusing aid, which consisted of seven aluminum rings (with diameters of 70 mm and intervals of 15 mm) supported by a Teflon tube, was positioned between the spinneret and the collecting plate. The rings were connected with seven resistors to obtain voltage gradient between adjacent rings when voltage was applied to the focusing aid. Positive voltages, generated by two high-voltage power supplies (DW-P103-1AC, Tianjin Dongwen, China), were respectively applied to the spinneret and the focusing aid, while a negative voltage was applied to the collecting plate.

Poly(vinyl pyrrolidone) (PVP, Mw = 130,000) solution with a weight concentration of 15% was prepared by dissolving PVP powders in ethanol and stirring by a magnetic stirrer for 2 hours. The PVP solution was pumped by a syringe pump (LSP04-1A, Longer Precision Pump Co., Baoding, China) and fed to the spinneret through a silicone rubber pipe at a flow rate of 8 μL/min. When high voltages were applied to the setup, a jet was ejected from the tip of spinneret and traveled along the central axis of rings to the collecting plate. The collecting plate was rotated by a servomotor and simultaneously driven by a computer-controlled translation stage to move along the radial direction. So the electrospun fibers were separated from each other and aligned on a silicon chip attached on the plate. The morphologies of fibers were characterized using a digital optical microscope (KH-1300, Hirox) and an environmental scanning electron microscope (ESEM, Quanta 200, FEI) with an accelerating voltage of 15 kV.

3 Electric field simulations

The electric field force is the dominant force applied to the jet, so the distribution and strength of the electric field greatly influence the shape and trajectory of the jet. Analyzing the electric field will provide a better understanding of the effect of the setup modification on the control of the jet path. The electric field distribution and strength on the central planes of the setups are calculated by the COMSOL software and shown in Fig. 2. The arrows indicate the direction of the electric field lines and the equipotential lines stand for the electric potentials. Figure 2(a) shows the simulation of the electric field when the upper plate is added to the setup to form a plate–spinneret–plate (P–S–P) system and voltages of +7000 and −2500 V are respectively applied to the upper and lower plates. The field lines near the central axis are almost parallel to each other except these at the initiating region of the setup. The divergence is mainly caused by the part of spinneret out of the upper plate. Although the electric field is uniformed for the introduction of the upper plate, the divergence of the electric field still exits and there is no horizontal constraint force applied to the jet. So the inherent bending instability cannot be eliminated in this system. Figure 2(b) illustrates the electric field distribution when the focusing aid is introduced to the setup to form a spinneret–focusing–plate (S–F–P) system. Voltages of +7000, +6000 and −2500 V are respectively applied to the spinneret, the focusing aid and the collecting plate. We can see that the field lines converge to the central axis at the lower part of the focusing aid. However, there is a considerable divergent tendency for the field lines from the tip of spinneret to the first two rings. The non-uniformity of the electric field in the initiating region may lead to the appearance of the bending instability and finally affect the stability

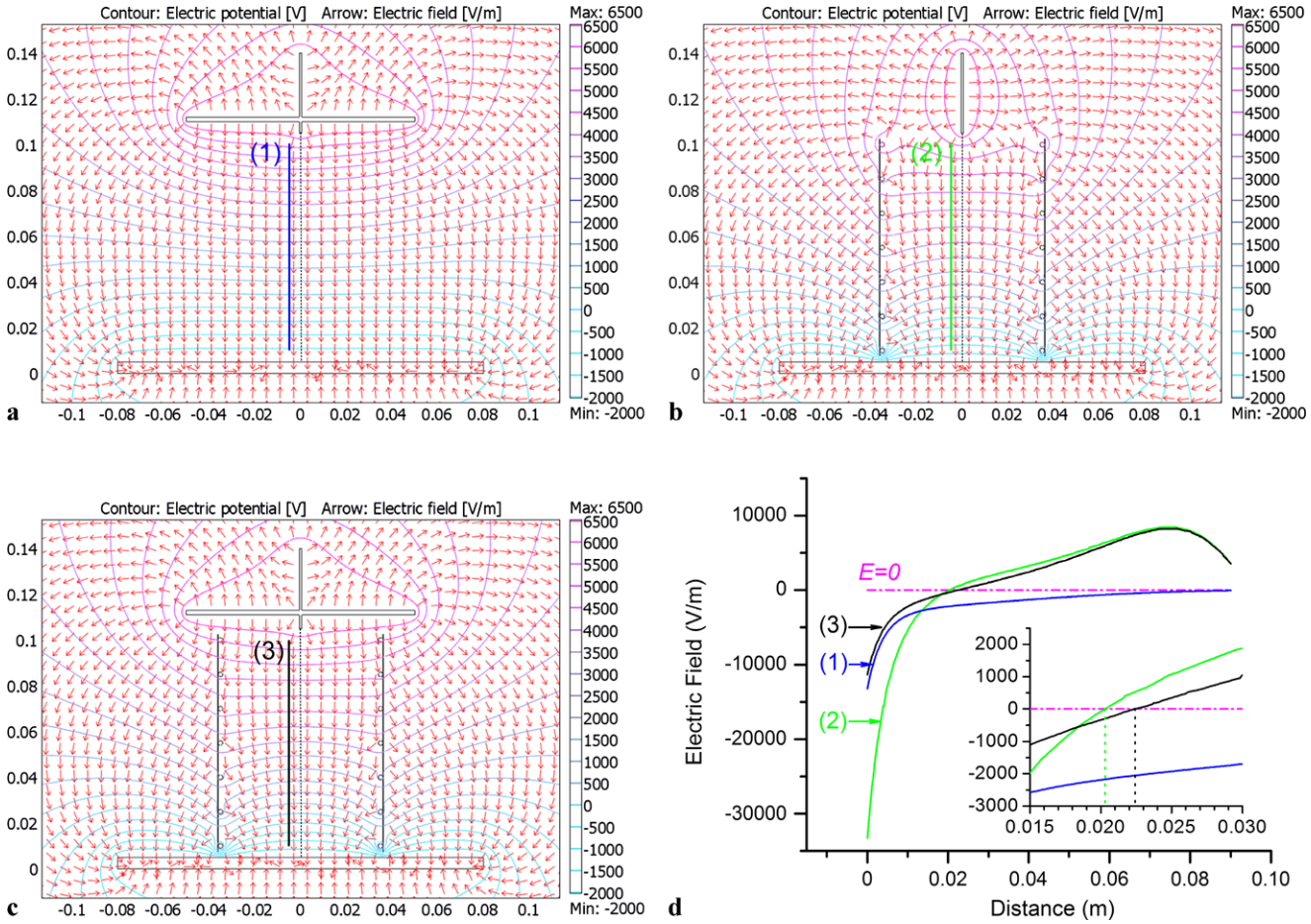

Fig. 2 The images of the simulated electric field distributions and the electric potential contours when (**a**) the upper plate, (**b**) the focusing aid, and (**c**) both the upper plate and focusing aid are introduced to the electrospinning setup. (**d**) The plot of the horizontal components of the electric field strength along the lines (1)–(3) which are 0.005 m away from the central axes of the setups and down from the height of 0.1 to 0.01 m. The *inset* shows the magnified image of the horizontal electric field near the zero-crossing point

of fiber deposition. Figure 2(c) shows the simulation of the electric field when a plate–spinneret–focusing–plate (P–S–F–P) system is formed by introducing both the upper plate and the focusing aid to the setup. It reveals that integrating the upper plate and the focusing aid into the conventional setup reduces the divergence of electric field at the initiating region and also leads to the formation of a convergent distribution of electric field at the lower part of the focusing aid.

The horizontal component of the electric field strength can quantitatively characterize the divergence of electric field. The horizontal component of electric field on lines (1)–(3) in the above three systems is calculated and plotted in Fig. 2(d). The electric field in the P–S–P system (on line (1)) is always divergent although the divergence gets smaller and smaller and close to zero. The electric field in the S–F–P system (on line (2)) changes direction and becomes convergent nearly at the middle of the second ring and the third one. However, the divergence of the electric field at the initiating region is much larger than that in the other two systems. The P–S–F–P system gathers the advantages of the first two systems. The electric field on the line (3) is uniformed at the initiating region and also becomes convergent nearly at the middle of the second ring and the third one. When the jet is perturbed at the initiating region of the P–S–F–P system, the perturbation has a tendency to develop into bending or whipping for the net repulsive electrostatic force applied to the jet. But after the jet passes through the middle of the second ring and the third one, the horizontal electric field force changes direction to point to the central axis, which restores the jet back to the central axis. Since the divergence of electric field is reduced by the upper plate and the beginning of continuous jet is immobilized by the tip of spinneret, the part of the jet at the initiating region may be stabilized by the fixation of restoring force and the downward acceleration of jet. So the setup integrated with the upper plate and the focusing aid provides a good possibility to suppress the jet bending

instability and precisely place the electrospun fibers on the substrate.

4 Results and discussion

In order to study the effect of the device modification on the configuration of the collected fibers, 15% PVP solutions are respectively electrospun in the above three systems. After high voltages are applied to the setup, a jet is ejected from the tip of spinneret and travels to the collecting plate. The collecting plate is rotated by a servomotor and the rotating velocity at the collecting position is 0.89 m/s. A computer-controlled translation stage is used to drive the whole collecting device moving along the radial direction of plate at a linear speed of 0.5–2 mm/s in order to avoid the overlap of the fibers. Figure 3 shows the SEM images and diameter distributions of the generated fibers when the upper plate, the focusing aid, and both of them are respectively introduced to the electrospinning setup. Figure 3(a) shows the PVP fibers generated from the P–S–P system. The deposition of the fibers is parallel to each other, but the architecture of the fibers is disordered and the lateral width of the fibrous band is not uniform and varies from about 100 to 200 μm. The depositing position is not fixed because of the swing of the jet. It means that the bending instability is not eliminated completely and the jet trajectory is not precisely controlled although it is reduced by the upper plate. Figure 3(b) shows the generated fibers when the PVP solution is electrospun in the S–F–P system. The structures of the deposited fibers become regular helical loops and the lateral widths of loops are limited in the range of 30–80 μm. The figure reveals that the spread of the jet path is limited by the convergent electric field force, but the bending instability is also not completely eliminated which affects the stability of the fiber deposition. Figure 3(c) illustrates the SEM image of fibers generated from the integrated P–S–F–P system. The deposited fibers are also restricted to become helical loops. The lateral widths of loops become more uniform and are reduced considerably to about 10 μm. The overlap of the fibers is mainly caused by the mismatch of the jet velocity and the collecting velocity. This demonstrates the jet trajectory is well controlled and the fibers are orderly laid on the substrate. The diameter distributions of the fibers obtained from the above three systems are shown in Fig. 3(d)–(f). The diameters of the fibers from the P–S–P system change from 1.096 to 1.518 μm and the average diameter is 1.277 μm. The diameters of the fibers generated from the S–F–P system vary from 1.002 to 1.635 μm and have an average value of 1.291 μm. Figure 3(f) displays the distribution of the fiber diameters for the P–S–F–P system. The fiber diameters are in the range of 1.934–2.546 μm and with an average value of 2.326 μm, which are about twice as large as these from the other two systems. The elongation of the jet in the P–S–F–P system is not sufficient in comparison with that in the other systems. This distinctly indicates that the jet does not undergo the bending or whipping process and only the stretching of the longitudinal electrostatic force is applied to the jet.

The effect of the collecting velocity on the morphology of PVP fibers is also studied. Figure 4(a)–(d) shows the optical microscope images of electrospun fibers separately collected at linear velocities of 0.89, 2.23, 4.92 and 6.70 m/s. The SEM images illustrate that the morphology of fibers is distinctly affected by the velocity of the rotating plate. Helical structures of fibers with closely overlapped loops are formed when the rotating velocity is low. This is because the collecting velocity cannot match the jet velocity. The loops are gradually drawn apart from each other as the collecting velocity increases and are finally straightened into parallel lines when the collecting velocity reaches 6.70 m/s.

The fibers diameter, lateral width and wavelength of the helical loops, as a function of the collecting velocity, are shown in Fig. 5. The wavelengths of loops increase from 3.65 ± 0.17 to 39.30 ± 1.45 μm, which are nearly proportional to the collecting velocity. The reason is that the depositing process is only affected by the relative motion between the substrate and the focusing aid since the operational parameters of electrospinning are fixed and the jet trajectory is restricted. The average diameters of the curved fibers range from 2.326 ± 0.163 to 2.427 ± 0.139 μm, while the value of the straight fibers is 2.036 ± 0.044 μm. The lateral widths are in the range of 7.77–11.83 μm, which are almost of the same order of magnitude as the diameters. We can see that the lateral widths of loops and diameters of fibers are insensitive to the variation of the collecting velocity. The fiber diameter is determined by the elongation of the jet, while the lateral width is determined by the oscillating range of the jet trajectory. The insensitivity of the diameter and the lateral width also reveals a good control of the jet bending instability in this system.

5 Conclusions

In conclusion, a focusing electric-field-assisted electrospinning method is demonstrated to be efficient for the steerable deposition of the PVP fibers. The bending instability of jet in the electrospinning process is eliminated due to the constraint of the focusing electric field force. Microfibers with helical structures are aligned on the rotating collector and the lateral widths of the helical fibers can be controlled within the magnitude of 10 μm. The morphologies of microfibers are conveniently adjusted from helical loops to straight lines by varying the collecting velocity. The ability

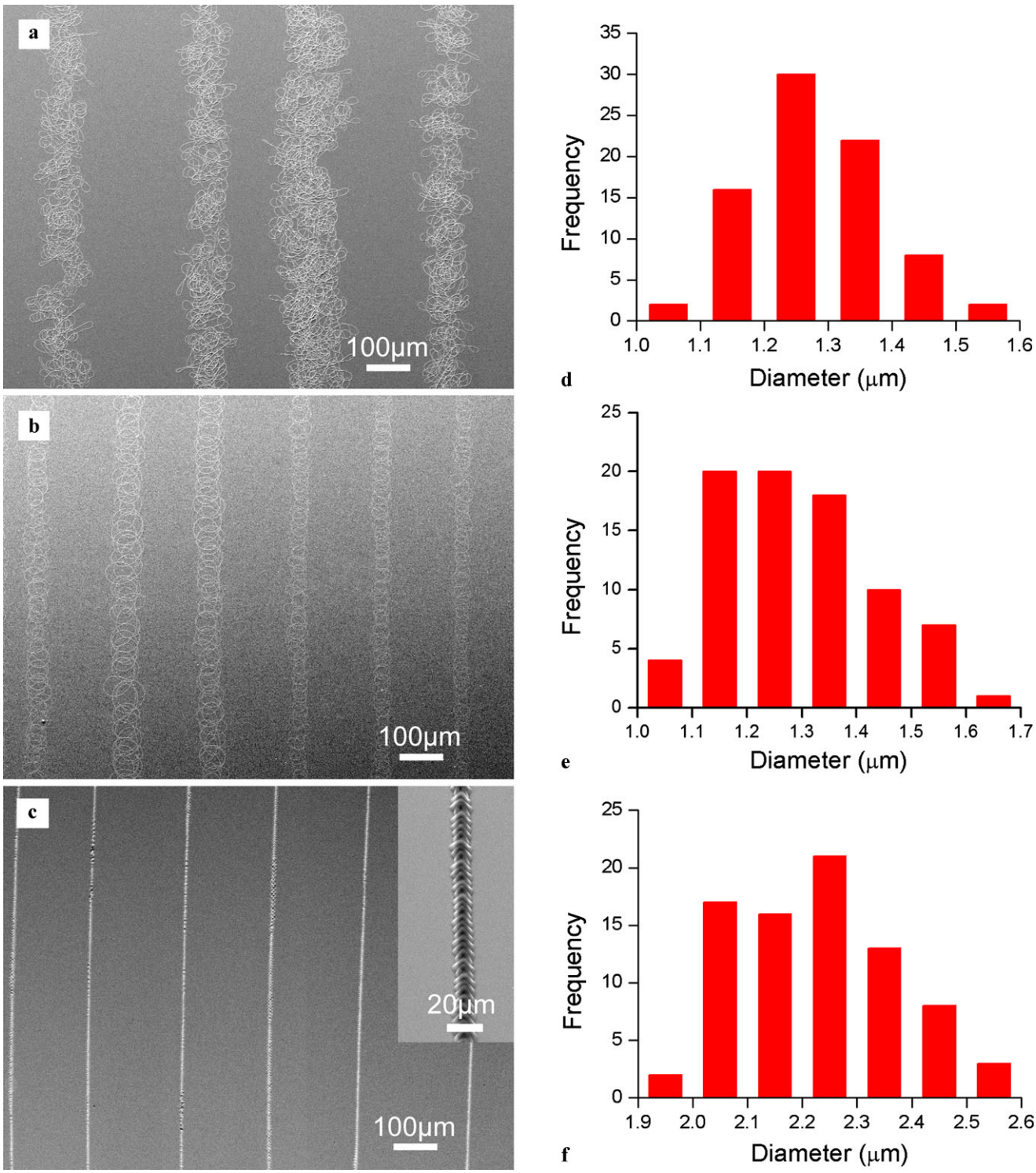

Fig. 3 The morphologies and the diameters of the fibers generated from different modified electrospinning systems. (**a**)–(**c**) SEM images of the fibers generated from (**a**) P–S–P system, (**b**) S–F–P system, (**c**) P–S–F–P system. The *inset* in (**c**) shows the magnified image of a single helical fiber. (**d**)–(**f**) The distribution histograms of the fibers diameters respectively shown in (**a**)–(**c**)

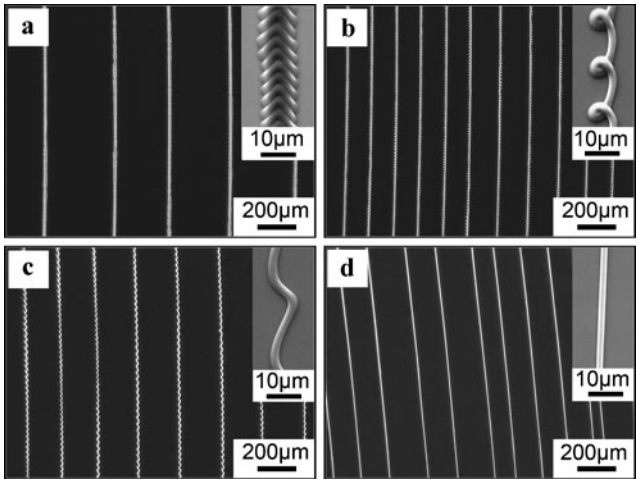

Fig. 4 (**a**)–(**d**) Optical microscope images of the electrospun fibers collected at linear velocities of 0.89, 2.23, 4.92 and 6.70 m/s, respectively. The *insets* show the SEM images of fibers at higher magnifications

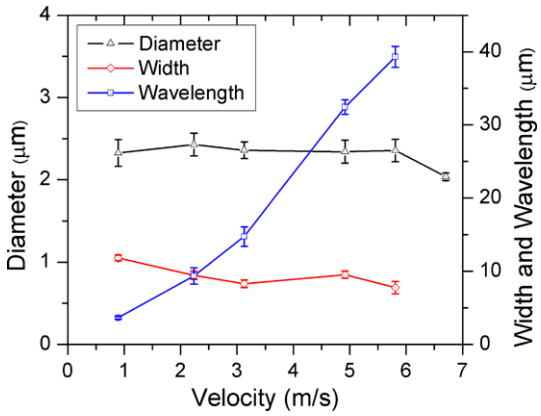

Fig. 5 Variations of the fiber diameter, the lateral width and wavelength of the helical loops with the increase of the collecting velocity (△ for the fiber diameter, ◊ for the lateral width and □ for the wavelength)

to precisely deposit the electrospun fibers provides a potential way for the fabrication of patterned polymer structures.

Acknowledgements This research is supported by the National High Technology R&D Program of China (Grant No. 2006AA02Z4E9) and the National Key Technology R&D Program of China (Grant No. 2006BAI03A18).

References

1. Z.M. Huang, Y.Z. Zhang, M. Kotaki, S. Ramakrishna, Compos. Sci. Technol. **63**, 2223 (2003)
2. D. Li, Y.N. Xia, Adv. Mater. **16**, 1151 (2004)
3. T. Subbiah, G.S. Bhat, R.W. Tock, S. Pararneswaran, S.S. Ramkumar, J. Appl. Polym. Sci. **96**, 557 (2005)
4. A. Greiner, J.H. Wendorff, Angew. Chem., Int. Ed. **46**, 5670 (2007)
5. D.H. Reneker, A.L. Yarin, H. Fong, S. Koombhongse, J. Appl. Phys. **87**, 4531 (2000)
6. Y.M. Shin, M.M. Hohman, M.P. Brenner, G.C. Rutledge, Polymer **42**, 9955 (2001)
7. Y.M. Shin, M.M. Hohman, M.P. Brenner, G.C. Rutledge, Appl. Phys. Lett. **78**, 1149 (2001)
8. Y. Dzenis, Science **304**, 1917 (2004)
9. M. Goldberg, R. Langer, X.Q. Jia, J. Biomater. Sci.-Polym. Ed. **18**, 241 (2007)
10. M.V. Kakade, S. Givens, K. Gardner, K.H. Lee, D.B. Chase, J.F. Rabolt, J. Am. Chem. Soc. **129**, 2777 (2007)
11. D.Z. Yang, J.F. Zhang, J. Zhang, J. Nie, J. Appl. Polym. Sci. **110**, 3368 (2008)
12. W.E. Teo, S. Ramakrishna, Nanotechnology **17**, R89 (2006)
13. H. Pan, L.M. Li, L. Hu, X.J. Cui, Polymer **47**, 4901 (2006)
14. E. Zussman, A. Theron, A.L. Yarin, Appl. Phys. Lett. **82**, 973 (2003)
15. D. Li, Y.L. Wang, Y.N. Xia, Nano Lett. **3**, 1167 (2003)
16. W.E. Teo, S. Ramakrishna, Nanotechnology **16**, 1878 (2005)
17. H. Lee, H. Yoon, G. Kim, Appl. Phys. A, Mater. Sci. Process. **97**, 559 (2009)
18. B. Sundaray, V. Subramanian, T.S. Natarajan, R.Z. Xiang, C.C. Chang, W.S. Fann, Appl. Phys. Lett. **84**, 1222 (2004)
19. C.Y. Xu, R. Inai, M. Kotaki, S. Ramakrishna, Biomaterials **25**, 877 (2004)
20. D.M. Zhang, J. Chang, Adv. Mater. **19**, 3664 (2007)
21. D.M. Zhang, J. Chang, Nano Lett. **8**, 3283 (2008)
22. Z.W. Ding, A. Salim, B. Ziaie, Langmuir **25**, 9648 (2009)
23. D.H. Sun, C. Chang, S. Li, L.W. Lin, Nano Lett. **6**, 839 (2006)
24. C. Chang, K. Limkrailassiri, L.W. Lin, Appl. Phys. Lett. **93** (2008)
25. C. Hellmann, J. Belardi, R. Dersch, A. Greiner, J.H. Wendorff, S. Bahnmueller, Polymer **50**, 1197 (2009)
26. J.M. Deitzel, J.D. Kleinmeyer, J.K. Hirvonen, N.C.B. Tan, Polymer **42**, 8163 (2001)
27. G.H. Kim, J. Polym. Sci. Part B, Polym. Phys. **44**, 1426 (2006)
28. L.M. Bellan, H.G. Craighead, J. Vac. Sci. Technol. B **24**, 3179 (2006)
29. A. Salim, C. Son, B. Ziaie, Nanotechnology **19** (2008)